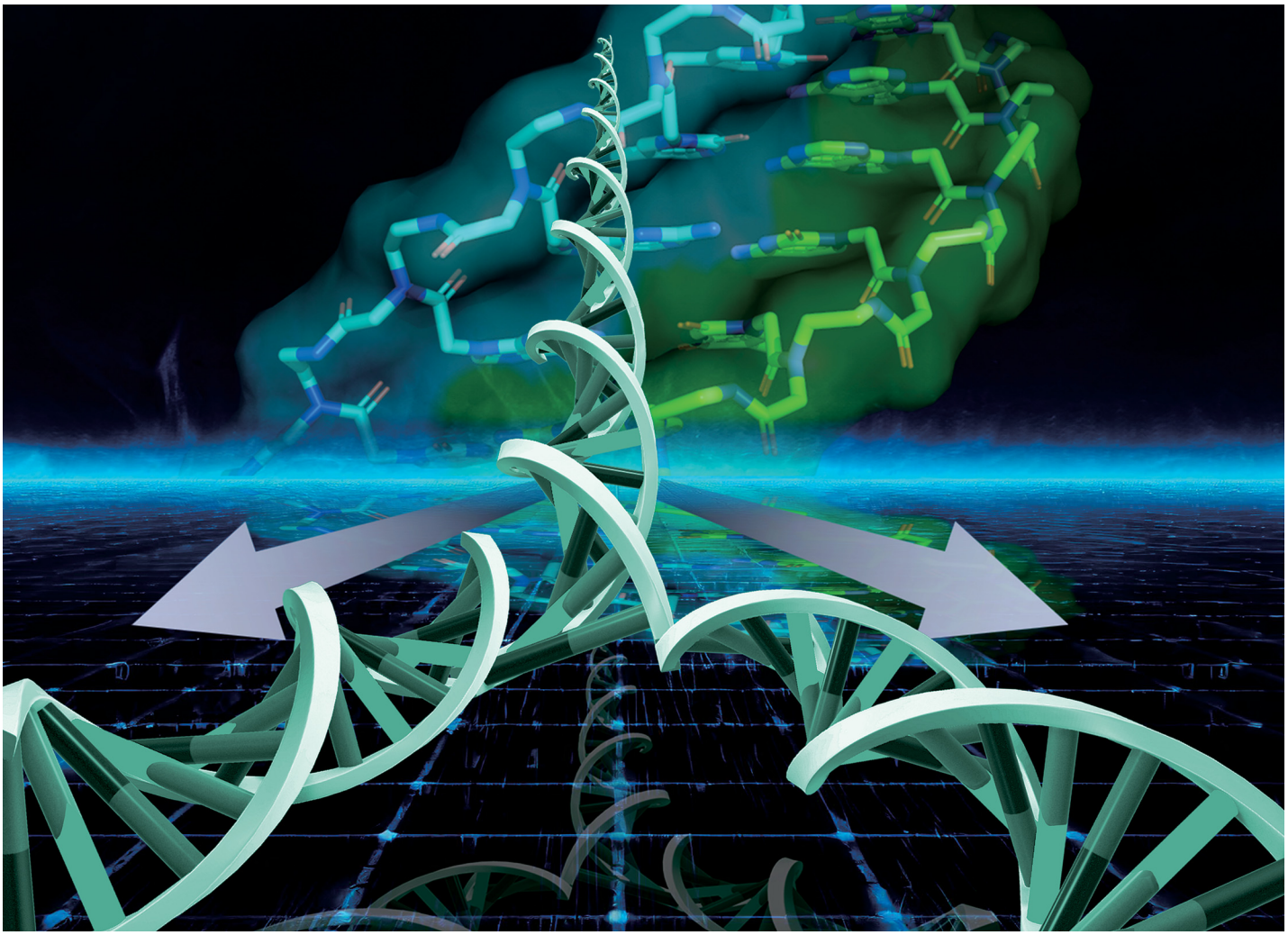

Showcasing research from Professor Shoji Osami's laboratory, Department of Chemistry, Graduate School of Science, Nagoya University, Nagoya, Japan.

Peptide nucleic acids in parallel orientation form invasion complexes with double-stranded DNA

This study explores the underutilized property of peptide nucleic acids (PNAs) to form parallel duplexes and introduces a novel double-duplex invasion strategy that takes advantage of parallel orientations, enabling recognition of specific target sequences in double-stranded DNA without requiring nucleobase modifications. The background illustrates the crystal structure of the parallel PNA/PNA duplex obtained in this work, and the arrows indicate the orientations of the parallel and antiparallel duplexes.

Image reproduced by permission of Masanari Shibata from *RSC Chem. Biol.*, 2025, **6**, 1566.

As featured in:

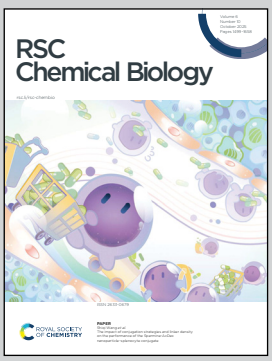

See Osami Shoji, Yuichiro Aiba *et al.*, *RSC Chem. Biol.*, 2025, **6**, 1566.

ROYAL SOCIETY OF CHEMISTRY

rsc.li/rsc-chembio

Registered charity number: 207890

RSC Chemical Biology

ROYAL SOCIETY OF CHEMISTRY

PAPER

View Article Online
View Journal | View Issue

Cite this: *RSC Chem. Biol.*, 2025, **6**, 1566

Peptide nucleic acids in parallel orientation form invasion complexes with double-stranded DNA

Masanari Shibata,[a] Hiroshi Sugimoto,[b] Masaki Hibino,[a] Osami Shoji*[a] and Yuichiro Aiba*[a]

Peptide nucleic acid (PNA) is a unique class of synthetic nucleic acids with a pseudo-peptide backbone, known for its high nucleic acid recognition capability and its ability to directly recognize double-stranded DNA (dsDNA) *via* the formation of a unique invasion complex. While most natural and artificial nucleic acids form duplexes in an antiparallel configuration due to the general instability of parallel configurations, PNA distinctively forms both antiparallel and parallel duplexes. In this study, we focused on this previously underexplored property of PNA to adopt a parallel duplex configuration and developed a novel double-duplex invasion strategy by leveraging the differences in thermal stability between the antiparallel and parallel orientations of PNA duplexes. Furthermore, we report the first crystal structure of a parallel PNA duplex, which was found to exhibit different structural features compared to the previously characterized antiparallel PNA duplex. This study highlights the potential of artificial nucleic acids in dsDNA recognition and demonstrates that the parallel architecture may serve as a conceptual foundation for advancing broader methodological innovations in nucleic acid research.

Received 3rd July 2025,
Accepted 20th August 2025

DOI: 10.1039/d5cb00172b

rsc.li/rsc-chembio

Introduction

Artificial nucleic acids are a class of chemically modified nucleic acid analogues, some of which exhibit properties superior to those of natural DNA and RNA. By incorporating modified nucleobases and/or backbones, artificial nucleic acids have expanded their applicability in biotechnology and nanotechnology, and have been widely utilized for nucleic acid recognition.[1–3] Among the various artificial nucleic acids, peptide nucleic acid (PNA) has been extensively studied[4,5] due to its exceptionally high binding affinity for DNA.[6–11] PNA features an electrostatically neutral pseudo-peptide backbone, in contrast to the negatively charged sugar-phosphate backbone of DNA (Fig. 1A).[6] As a result, there is no electrostatic repulsion between PNA and the phosphate backbone of DNA, contributing to stable duplex formation of PNA with DNA than the equivalent DNA/DNA duplex (Fig. 1B; preorganization of the PNA backbone also play a role in this enhanced stability).[12,13] Among the various artificial nucleic acids developed to date, PNA exhibits one of the strongest DNA-binding affinities. Notably, PNA also displays unique binding modes that are not commonly observed in other synthetic analogues, including the ability to directly recognize double-stranded DNA (dsDNA). These include duplex invasion,[14–20] triplex invasion,[6,21–29] and double-duplex invasion (Fig. 1C).[8,9,30,31] In these binding modes, invasion complexes are formed through the sequence-specific hybridization of PNA strands with complementary sequences within dsDNA. Among the types of invasion complexes, double-duplex invasion can recognize sequences with mixed nucleobase compositions. In this mode, two PNA strands, each designed to be complementary to one strand of the target dsDNA, invade the dsDNA and form two separate PNA/DNA duplexes, as illustrated in Fig. 1C.[30,31]

In addition to its ability to form invasion complexes, PNA exhibits another distinctive feature in duplex-forming behavior that sets it apart from other artificial nucleic acids: strand

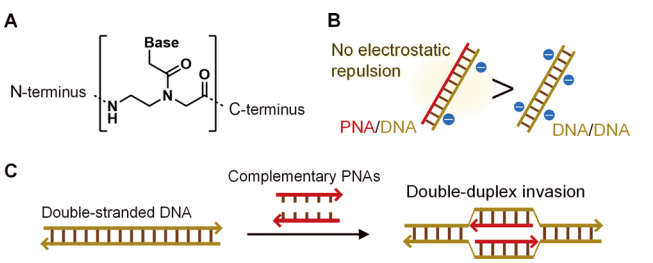

Fig. 1 (A) Chemical structure of peptide nucleic acid (PNA). (B) Comparison of thermal stability between PNA/DNA and DNA/DNA duplexes. (C) Unique DNA recognition by PNA *via* double-duplex invasion complex formation.

[a] *Department of Chemistry, Graduate School of Science, Nagoya University, Furo-cho, Chikusa-ku, Nagoya, 464-8602, Japan. E-mail: aiba.yuichiro.f4@f.mail.nagoya-u.ac.jp; Fax: +81-52-789-3557; Tel: +81-52-789-2953*

[b] *RIKEN SPring-8 Center, 1-1-1 Kouto, Sayo, Hyogo, 679-5148, Japan*

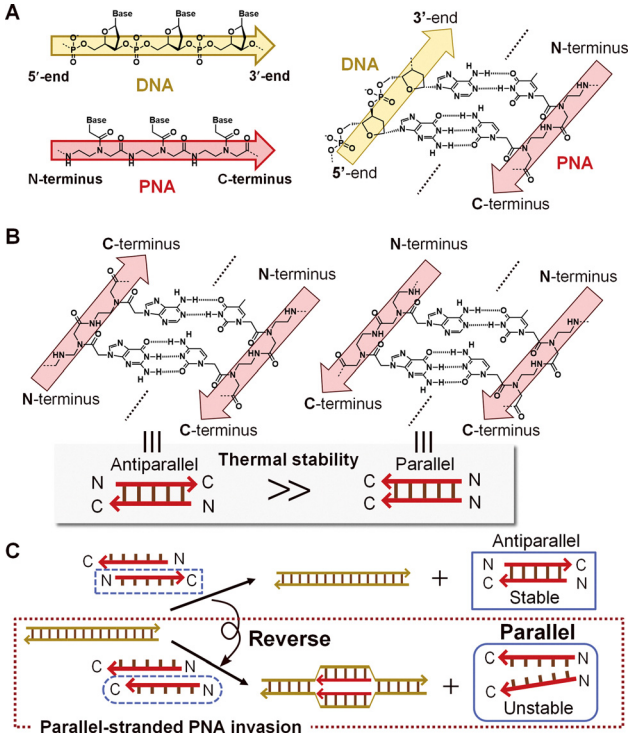

Fig. 2 (A) Schematic representation of the strand orientation of DNA and PNA (left), and their relative alignment in antiparallel DNA/PNA duplex (right). (B) Orientation of each strand in antiparallel (N → C/C ← N) and parallel (N → C/N → C) PNA/PNA duplexes. The parallel PNA/PNA duplex is much less stable than the corresponding antiparallel PNA/PNA duplex. (C) Our parallel-stranded PNA invasion system: The use of parallel-stranded PNAs inhibits undesirable PNA/PNA duplex formation and enables the formation of invasion complex without the need for chemically modified PNAs. N and C stand for the N- and C-termini of PNA, respectively.

orientation flexibility. In nature, dsDNA typically adopts an antiparallel configuration, where the two DNA strands run in opposite directions, with the 5′-end of one strand aligned with the 3′-end of the other strand. Analogously, a PNA strand possesses an N-terminus and a C-terminus, corresponding to the 5′- and 3′-ends of DNA, respectively (Fig. 2A). Interestingly, DNA and PNA can form two distinct duplex orientations, parallel and antiparallel, even when the nucleobase sequence is identical. Remarkably, PNA can form stable duplexes with complementary DNA in both antiparallel and parallel orientations,[12] a property rarely observed in natural or artificial nucleic acids. However, parallel duplexes tend to be less thermodynamically stable than their antiparallel counterparts.

As a result, the potential of this parallel binding mode has remained underexplored in previous research, which has primarily focused on enhancing binding strength and duplex stability. Herein, we demonstrated that the parallel orientation, which is recognized but not extensively investigated, can play a critical role when reconsidered from a different perspective, offering a new conceptual strategy for the formation of invasion complexes.

Double-duplex invasion requires not only a high binding affinity of PNA for DNA, but also the suppression of PNA/PNA self-duplex formation. This requirement arises from the fact that the two PNA strands used for invasion are inherently complementary to each other, and PNA/PNA duplexes are generally more stable than the corresponding PNA/DNA duplexes.[32] Consequently, self-duplex formation competes with invasion complex formation, as the PNA strands preferentially hybridize with each other rather than with the target DNA strands. To overcome this challenge, pseudo-complementary PNAs (pcPNAs),[15,30,33] in which adenine (A) and thymine (T) are substituted with 2,6-diaminopurine (D) and 2-thiouracil (Us), respectively, have been extensively utilized. This substitution induces steric repulsion between the amino group of D and the thione group of Us, significantly destabilizing duplex formation between complementary pcPNA strands (Fig. S1), while still permitting the formation of stable pcPNA/DNA duplexes during invasion into dsDNA (Fig. 1C). As an alternative strategy, we propose exploiting the unique ability of PNA to adopt both antiparallel and parallel strand orientations. Notably, there is a pronounced difference in thermal stability between antiparallel and parallel PNA/PNA duplexes, with the parallel configuration being markedly less stable than its antiparallel counterpart (Fig. 2B). By capitalizing on this unique property, we hypothesized that designing two PNA strands in parallel orientation, as illustrated in Fig. 2C, would significantly suppress unintended PNA/PNA duplex formation, thereby facilitating invasion into dsDNA.

In addition, we have determined the first crystal structure of the parallel PNA/PNA duplex. To deepen the understanding of the parallel PNA/PNA duplex, which has not been well characterized, we have compared it with the antiparallel duplex reported previously.[34,35]

Results and discussion

PNA oligomer design and synthesis

We designed PNA oligomers in both antiparallel and parallel orientations. All PNA oligomers contained a free N-terminal amino group, while the C-terminal carboxylic acid was amidated. To enhance water solubility of PNAs, lysine residues, positively charged under neutral pH conditions, were attached to the N- and/or C-termini. Twenty-seven PNA oligomers were synthesized using Fmoc-PNA monomers on an automated solid-phase peptide synthesizer. Three pseudo-complementary PNA oligomers were synthesized manually using Boc-PNA monomers. The sequences of these oligomers are listed in Table S1.

Hereafter, PNAs will be referred to as either antiparallel (apsPNA) or parallel (psPNA) based on the strand orientation of the duplex formed with PNA-Fw (Fig. 3A and C). Herein, PNA-Fw is defined as the PNA strand complementary to the target sequence in the upper DNA strand in Fig. 3B. Consequently, PNA/DNA duplexes formed between DNA and either PNA-Fw or apsPNAs are antiparallel in orientation, whereas those formed between DNA and psPNAs adopt a parallel orientation (Fig. 3B).

Formation of an invasion complex with parallel-stranded PNAs

The formation of an invasion complex was confirmed by electrophoretic mobility shift assay (EMSA) using a microchip

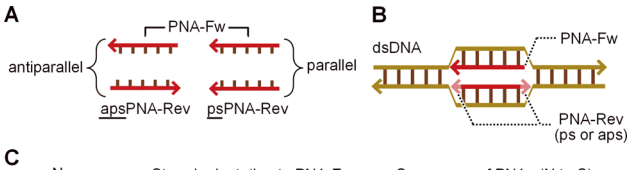

C

Name	Strand orientation to PNA-Fw	Sequences of PNAs (N to C)
PNA-Fw	–	*K*ATGACTAAGAGTAGT*KK*
apsPNA-Rev	antiparallel	*K*ACTACTCTTAGTCAT*KK*
psPNA-Rev	parallel	*K*TACTGATTGTCATCA*KK*

Fig. 3 Schematic representation of (A) the strand orientation of PNAs and (B) the invasion complex. (C) A summary of the PNA sequences used in the invasion experiments. 'aps' and 'ps' denote the strand orientation of each PNA relative to the complementary PNA-Fw strand in the duplex, representing antiparallel and parallel orientations, respectively. Lysine (*K*) residues were introduced at the termini of the PNAs to improve water solubility.

electrophoresis system, which is similar to capillary electrophoresis rather than gel electrophoresis. This method can provide results consistent with native PAGE.† To facilitate the analysis of invasion complex formation based on electrophoretic mobility, a 119-bp dsDNA fragment was prepared by PCR using the pBFP-N1 plasmid as a template and employed as the target.

The invasion complex can be observed as a band with a different electrophoretic mobility compared to unbound dsDNA, reflecting structural alterations in the dsDNA at the invasion site.[36] Adding PNA-Fw and apsPNA-Rev to a solution containing target 119-bp dsDNA (Fig. 4A) only yielded a single band corresponding to the target dsDNA, even when excess amounts of PNAs were added (Fig. 4B; lanes 2–5). This result clearly shows that, in the absence of modified nucleobases (*i.e.*, pcPNA), a pair of antiparallel-stranded PNAs cannot form the invasion complex. The observation indicates that PNA-Fw and apsPNA-Rev preferentially form a stable antiparallel PNA/PNA duplex, decreasing the effective concentration of PNA strands available for invasion. In contrast, the combination of PNA-Fw and psPNA-Rev, which forms a thermodynamically less stable parallel PNA/PNA duplex, resulted in a new lower-mobility band with the target dsDNA (Fig. 4B; lanes 6–8). Moreover, the band became more intense with increasing equivalents of PNA (lane 6, 13.4 ± 2.2%; lane 7, 51.8 ± 3.3%; lane 8, 65.0 ± 3.3%). These results suggest that parallel-stranded PNAs interact with dsDNA to form a complex.

To confirm that the lower-mobility band was formed by two types of PNA strands (PNA-Fw and psPNA-Rev), 5-carboxyfluorescein (FAM) was attached to the N-termini of the PNAs (Fig. 4C). When one or both of the PNAs were replaced by FAM-labeled ones (Fig. 4C left; lanes 4–6), a lower-mobility band appeared at the same position as lane 3 across all lanes. Fluorescence emission was detected from the low-mobility bands in all cases (Fig. 4C right; lanes 4–6), indicating that these bands contained the PNAs. Interestingly, FAM labeling of PNA-Fw enhanced invasion efficiency (Fig. 4C left; lane 4), whereas FAM labeling of PNA-Rev reduced it (Fig. 4C left; lane 5). Previous research on Ru-complex-modified pcPNAs demonstrated that the introduction position of the Ru complex and the linker structure significantly affect invasion efficiency.[37] Given this, the structural difference between antiparallel (PNA-Fw_FAM) and parallel (psPNA-Rev_FAM) PNA/DNA duplexes may lead to a phenomenon similar to that observed for the Ru complex. Based on these results, we concluded that both Fw and Rev PNAs interact with dsDNA and form an invasion complex. In contrast, when only one of the two PNA strands was mixed with target dsDNA, no band shift was observed (Fig. S2), demonstrating that this dsDNA recognition requires the cooperative action of both PNA-Fw and psPNA-Rev. These findings support the conclusion that two parallel-stranded PNAs interact with dsDNA to form an invasion complex as intended.

To confirm that the PNA forms an invasion complex through accurate sequence recognition, a point mutation was introduced at the center of the parallel-stranded PNA pair, resulting in a single base-pair mismatch at the position highlighted in Fig. 4D. The parallel-stranded PNAs efficiently formed an invasion complex with fully complementary target dsDNA (lane 3). However, in the presence of a single base-pair mismatch between the PNA and the target DNA, no band corresponding to the invasion complex was observed, regardless of the mismatch combination (lanes 4–6). These results indicate that only PNAs with full sequence complementary to the target dsDNA are capable of forming invasion complexes, thereby supporting the formation of the intended double-duplex invasion structure. From the perspective of specific dsDNA recognition, the ability to discriminate between target and non-target sequences with high selectivity is essential. Among various types of mismatches, G–T and T–T mismatches are known to be relatively stable and often reduce sequence selectivity.[38–41] In contrast, our invasion system using parallel-stranded PNAs successfully discriminated single mismatches even when the target DNA contained thermodynamically stable mismatches such as G–T and T–T (lanes 4 and 6). These findings underscore the high sequence selectivity of our parallel-stranded PNA invasion system and confirm that the observed complex is indeed the intended double-duplex invasion complex.

Differences in thermal stability between PNA/PNA and PNA/DNA duplexes enhancing the formation of invasion complex

To better understand the mechanism governing the newly developed parallel-stranded PNA invasion system, we measured the melting temperature (T_m) values of antiparallel and parallel PNA/PNA and PNA/DNA duplexes (Fig. 5A). For this experiment, we used 15-mer single-stranded PNAs and DNAs, each corresponding to the target dsDNA sequences. As expected, a very low T_m value was obtained for the parallel PNA/PNA duplex (Fig. 5B; bar 2, PNA-Fw/psPNA-Rev, 62 °C) compared with the antiparallel PNA/PNA duplex (bar 1, PNA-Fw/apsPNA-Rev, over 90 °C). In the case of PNA/DNA duplexes, all antiparallel (bar 3,

† At first glance, it may appear that the samples were not run on the same gel, making lane comparison challenging (see Fig. 4B). However, by using the relative mobility of specific markers, equivalent results can be obtained as if the samples were run in parallel on the same gel, ensuring the analysis is reliable.

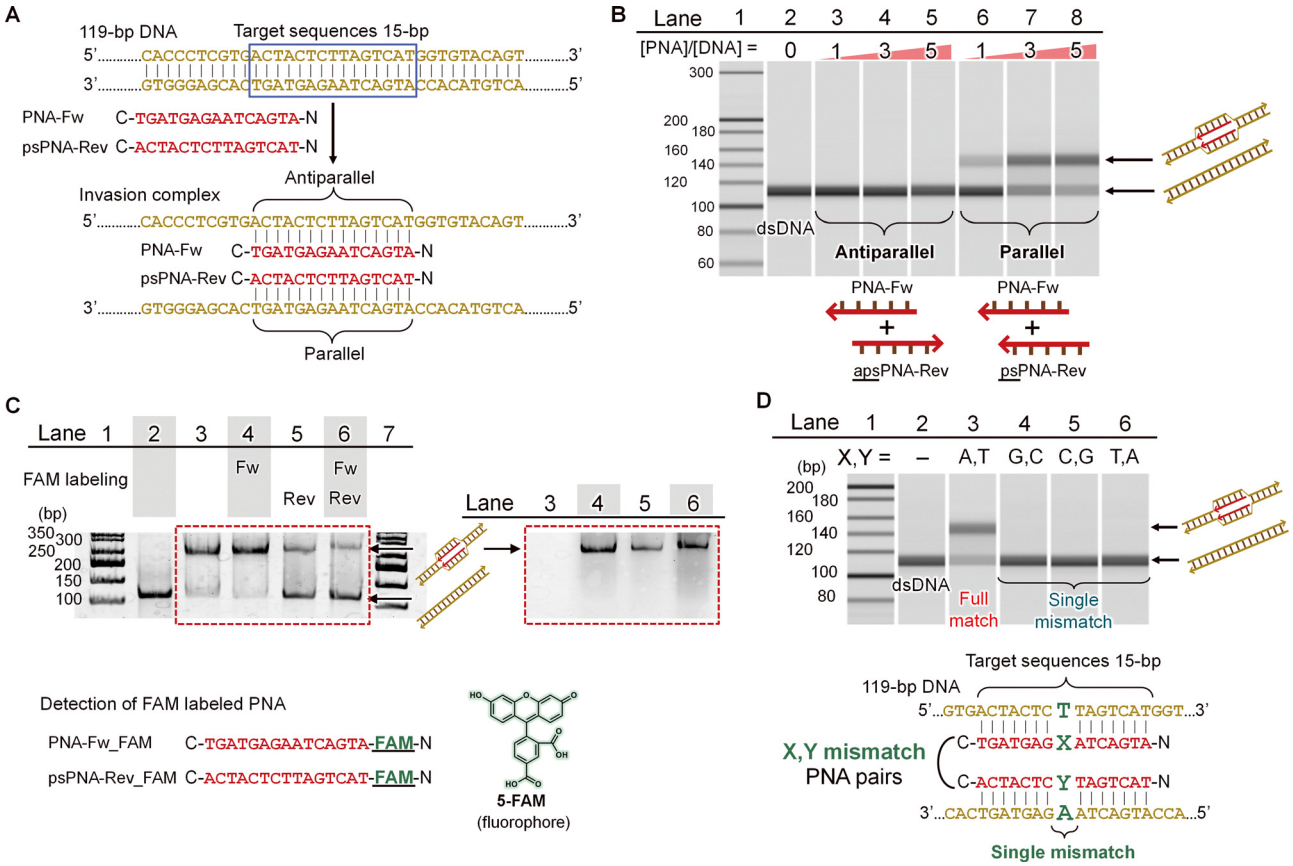

Fig. 4 (A) Overview of invasion complex formation between target 119-bp dsDNA and parallel-stranded PNAs. PNA-Fw and PNA-Rev hybridize to DNA strands in antiparallel and parallel orientations, respectively, forming the invasion complex. (B) Electrophoretic mobility shift assay (EMSA) shows that parallel-stranded PNA pairs form an invasion complex. Lane 1: 20-bp DNA ladder marker; lane 2: 119-bp target DNA only; lanes 3–5: PNA-Fw and apsPNA-Rev; lanes 6–8: PNA-Fw and psPNA-Rev. Invasion conditions: [DNA] = 100 nM, [each PNA] = 100–500 nM (1–5 equiv. for DNA), and [HEPES (pH 7.0)] = 5 mM at 50 °C for 1 h. (C) EMSA confirmed the presence of PNA in the invasion complex. FAM-labeled PNAs were used to detect PNA by fluorescent emission of 5-carboxyfluorescein (FAM). The bands of dsDNA and invasion complex were stained with GelRed™ (Biotium) (Ex. 532 nm/Em. 575 nm, left) and PNAs were detected by fluorescein labeling (Ex. 473 nm/Em. 510 nm, right). Lanes 1, 7: 50-bp DNA ladder marker; lane 2: 119-bp dsDNA only; lane 3: PNA-Fw and psPNA-Rev; lane 4: PNA-Fw_FAM and psPNA-Rev; lane 5: PNA-Fw and psPNA-Rev_FAM; lane 6: PNA-Fw_FAM and psPNA-Rev_FAM. Invasion conditions: [119-bp dsDNA] = 100 nM, [each PNA] = 500 nM, [HEPES (pH 7.0)] = 5 mM at 50 °C for 1 h. (D) Evaluation of the sequence selectivity of the parallel-stranded PNA invasion system. Lane 1: 20-bp DNA ladder marker; lane 2: 119-bp DNA only; lane 3: PNA-Fw and psPNA-Rev; lane 4: G,C mismatch pair (X = G, Y = C); lane 5: mismatch C,G pair (X = C, Y = G); lane 6: mismatch T,A pair (X = T, Y = A). Invasion conditions: [DNA] = 100 nM, [each PNA] = 500 nM (5 equiv. for DNA), and [HEPES (pH 7.0)] = 5 mM at 50 °C for 1 h.

PNA-Fw/compDNA-Rev, 83 °C; bar 4, compDNA-Fw/apsPNA-Rev, 76 °C) and parallel (bar 5, compDNA-Fw/psPNA-Rev, 68 °C) duplexes showed substantially higher T_m values than the corresponding DNA/DNA duplex (compDNA-Fw/compDNA-Rev, 27 °C). Moreover, both PNA/DNA duplexes related to invasion complex formation (bar 3, PNA-Fw/compDNA-Rev, 83 °C; bar 5, compDNA-Fw/psPNA-Rev, 68 °C) were more stable than the corresponding parallel PNA/PNA duplex (bar 2, PNA-Fw/psPNA-Rev, 62 °C).

From these results, it is evident that antiparallel-stranded PNAs form highly stable PNA/PNA duplexes, hindering efficient binding to the target DNA (Fig. 5C top). In contrast, designing PNAs in parallel orientation reverses the relative thermal stability between PNA/PNA and PNA/DNA duplexes. In the case of parallel-stranded PNAs, binding preferentially occurs between PNA and the target DNA, as the PNA/DNA duplexes exhibit greater stability than the corresponding parallel PNA/PNA duplex (Fig. 5C bottom). This preference arises from the reduced stability of the undesired PNA/PNA duplex in the parallel orientation compared to its antiparallel counterpart. Therefore, we concluded that the difference in thermal stability between PNA/PNA and PNA/DNA duplexes, specifically the higher stability of parallel PNA/DNA duplexes than parallel PNA/PNA duplexes, drives the favorable formation of the target invasion complex.

Structural characteristics of parallel PNA/PNA duplex compared to antiparallel PNA/PNA duplex

In the context of the structural polymorphism of nucleic acids, far fewer studies have been conducted on parallel duplexes than antiparallel ones. Similarly, for PNA, crystallographic analyses of PNA/PNA duplexes have been limited to antiparallel structures. Here, we report the first X-ray crystal structure of a parallel PNA/PNA duplex. Two strands of 8-mer PNAs designed

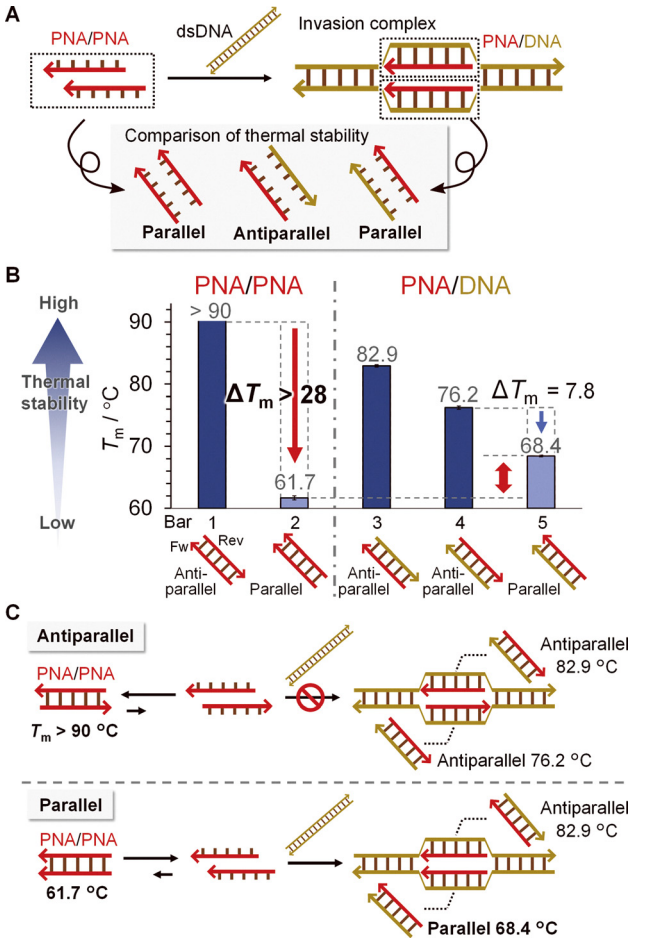

Fig. 5 (A) Thermal stability of PNA/PNA and PNA/DNA duplexes, measured as representative partial structures of the invasion complex due to the difficulty of direct assessment. (B) Melting temperatures (T_m) of PNA/PNA (bars 1, 2) and PNA/DNA (bars 3–5) duplexes to evaluate their thermal stability. T_m values are shown above the corresponding bars. Bar 1; PNA-Fw/apsPNA-Rev; bar 2; PNA-Fw/psPNA-Rev; bar 3; PNA-Fw/compDNA-Rev; bar 4; compDNA-Fw/apsPNA-Rev; bar 5; compDNA-Fw/psPNA-Rev. Conditions: [each strand of DNA or PNA] = 1 μM and [HEPES (pH 7.0)] = 5 mM. (C) Schematic illustration of states involved in invasion complex formation for antiparallel- (top) and parallel-stranded PNAs (bottom).

in parallel orientation were prepared (Xtal PNA-Fw and Xtal PNA-Rev) and crystallized in a 1 : 1 complex. X-ray crystallographic analysis revealed the structure of the parallel PNA/PNA duplex at 1.7 Å resolution (PDB ID: 9L5Z, Table S2). Two right-handed helices and two left-handed helices comprise the asymmetric unit, with alternating stacking of right- and left-handed helical duplexes in the crystals (Fig. S3). All nucleobases formed standard Watson–Crick base pairs, and the helical parameters were similar to those of the antiparallel PNA/PNA duplex (Table S3).[35] Interestingly, the macroscopic structures of the parallel and the antiparallel duplexes were very similar, even though one strand is inverted (Fig. 6A).[35] Various previous studies have reported that the carbonyl group in the linker connecting the nucleobase and the backbone is oriented towards the C-terminus of the PNA strands in the antiparallel duplex.[34,35,42] In contrast, in the parallel duplex presented here, the carbonyl group was found to be oriented towards the C-terminus in one strand and towards the N-terminus in the other strand (Fig. 6B). This results in differing relative positions of the nucleobases and the backbone amide groups between the two strands, which is a difference not observed in the antiparallel duplex. Moreover, a marked difference in the coordination of surrounding water molecules was observed between the two strands in the parallel duplex. In the 'C═O → C-terminus' strand (green strand in Fig. 6B), water molecules directly bridge the amide groups in the backbone and the nucleobases, which is consistent with previous observation in antiparallel PNA/PNA duplexes.[34,35] In contrast, in the 'C═O → N-terminus' strand (cyan strand in Fig. 6B), the number of bridging water molecules was clearly reduced, as shown in Fig. 6C and D (6 for the 'C═O → C-terminus' strand *vs.* 2 for the 'C═O → N-terminus' strand). The difference in the relative positions of the nucleobases and the amide groups, observed in the parallel duplex, may significantly influence the coordination of bridging water molecules. Based on previous studies suggesting that coordinating water molecules contribute to the stability of PNA/PNA duplexes,[43] the observed hydration pattern is likely a key factor in elucidating the reduced thermal stability of the parallel PNA/PNA duplex, which remains unclear.

Systematic evaluation of parameters governing parallel-stranded PNA invasion

To understand the basic characteristics of this new invasion system, we investigated (I) the effect of PNA oligomer length, (II) sequence flexibility, (III) kinetics, and (IV) temperature dependence (Fig. S4). Regarding the relationship between invasion efficiency and PNA oligomer length, 11-mer and 12-mer parallel-stranded PNAs were designed based on the sequences of 15-mer PNAs used in the earlier experiments in this study. These shorter PNAs were synthesized on a peptide synthesizer following the same protocol as for 15-mer PNAs and were evaluated by EMSA (Table S1 and Fig. S5). Although their invasion efficiency was lower than that of the 15-mer PNAs, the formation of an invasion complex was possible even with the shorter parallel-stranded PNAs.

Subsequently, we examined whether our parallel-stranded PNA system is available for different target sequences. We designed three additional sets of parallel-stranded PNAs (Fig. 7; GC-rich PNA-Fw_1/GC-rich psPNA-Rev_1, GC-rich PNA-Fw_2/GC-rich psPNA-Rev_2, and GC-rich PNA-Fw_3/GC-rich psPNA-Rev_3) targeting sequences with nucleotide compositions distinct from the previously tested AT-rich sequence (Fig. 4, AT ratio; 10/15). These newly synthesized parallel-stranded PNAs successfully recognized their target dsDNA and formed invasion complexes even with different sequences. These results demonstrate that recognition by the parallel-stranded PNA system is not limited to AT-rich sequences, and that invasion complexes can be formed even in highly GC-rich targets (Fig. 7C, GC ratio; 10/15). The efficiency of invasion complex formation with the GC-rich sequences was lower than that with the AT-rich sequence (Fig. 7A; lane 3, 10.4 ± 1.7%; lane 4, 23.9 ± 1.6%; Fig. 7B; lane 3, 5.7 ± 0.4%; lane 4,

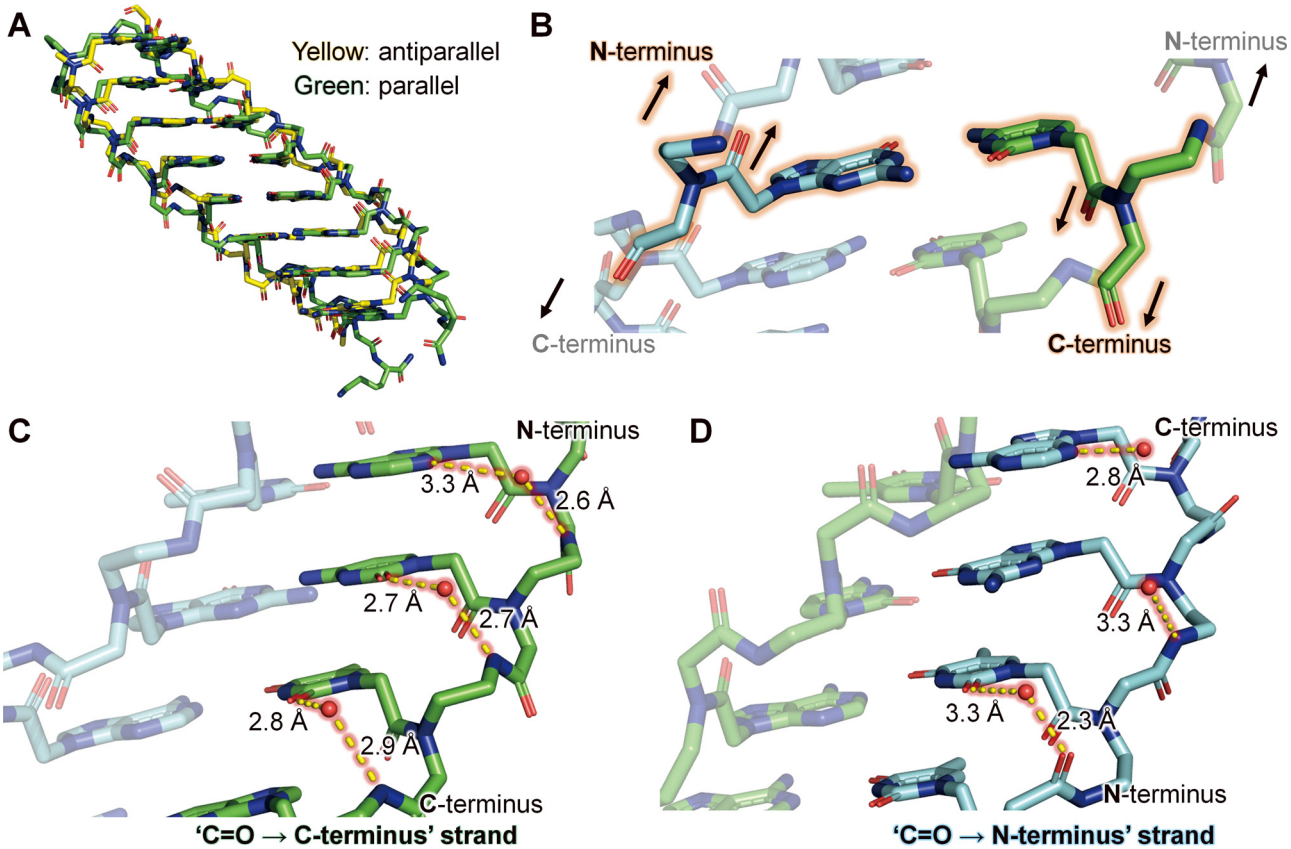

Fig. 6 X-ray crystal structure of parallel PNA/PNA duplex. (A) Superposition of 8-bp antiparallel PNA/PNA duplex (yellow, PDB ID: 3MBS) and 8-bp parallel PNA/PNA duplex (green, this work, PDB ID: 9L5Z). (B) Two types of backbone conformation in the parallel duplex. (C) In the strand of 'C═O → C-terminus' (green), the backbone amide groups are involved in the water-mediated hydrogen bond that bridges the backbone and nucleobase. (D) In the strand of 'C═O → N-terminus' (cyan), the backbone carbonyl groups are involved in the water-mediated hydrogen bond. The water molecules within 3.3 Å of polar atoms are depicted as red spheres and hydrogen bonds are depicted as yellow dashed lines with distances.

10.4 ± 0.6%; Fig. 7C; lane 3, 7.0 ± 1.6%; lane 4, 10.0 ± 3.0%), likely due to the higher thermodynamic stability of GC-rich DNA duplexes. Efficient recognition of GC-rich sequences has long been one of the major challenges in PNA invasion.[44–47] The ability of parallel-stranded PNAs to accurately recognize sequences with widely different nucleobase compositions represents a significant advance in the field.

To provide further insight into the kinetic properties of invasion complex formation using parallel-stranded PNAs, we conducted a time-course analysis to monitor the formation over time. The experiments were performed under the previously described conditions (5 equivalents of 15-mer PNAs with 100 nM 119-bp dsDNA at 50 °C), while varying the incubation times. As shown in Fig. 8A, the invasion complex formation with parallel-stranded PNAs progressed over time and reached a plateau around 50 minutes. Assuming that the formation of the invasion complex by parallel-stranded PNAs follows pseudo-first-order kinetics, the pseudo-first-order rate constant for PNA invasion, k_{ps}, was calculated from the slope of a plot of $-\ln(1 - C)$ *vs.* incubation time, where C is the fraction of the invasion complex at time t (Fig. 8B). Compared to the previously reported time-course data for invasion complex formation by pcPNA at 45 °C,[31] the slope for the parallel-strand PNA at the higher temperature of 50 °C appears to be less steep. Since a larger rate constant k_{ps} is typically expected at a higher temperature, this suggests that parallel-stranded PNAs form invasion complexes at a slower rate than pcPNAs. This slow formation of the invasion complex probably results from the slow binding of parallel-stranded PNA to its complementary DNA.[48] Because we cannot directly observe the binding of parallel-stranded and antiparallel-stranded PNAs to DNA during the invasion process, we evaluated their binding to single-stranded DNA. Here, we used the PNAs that were employed in the invasion experiments, along with their complementary single-stranded DNAs (Fig. S6A). The rates of antiparallel and parallel PNA/DNA duplex formation were evaluated by monitoring the decrease in single-stranded DNA bands during electrophoresis. The antiparallel PNA strand completed duplex formation within ten minutes (Fig. S6B), whereas the parallel PNA strand required one to two hours to complete duplex formation (Fig. S6C). We conclude that the formation of parallel duplexes is kinetically less favorable than that of antiparallel duplexes with the PNAs used in this study. This observation is consistent with an early report on the binding properties of PNA to complementary DNA.[48] These results suggest that the invasion process of parallel-stranded PNAs is

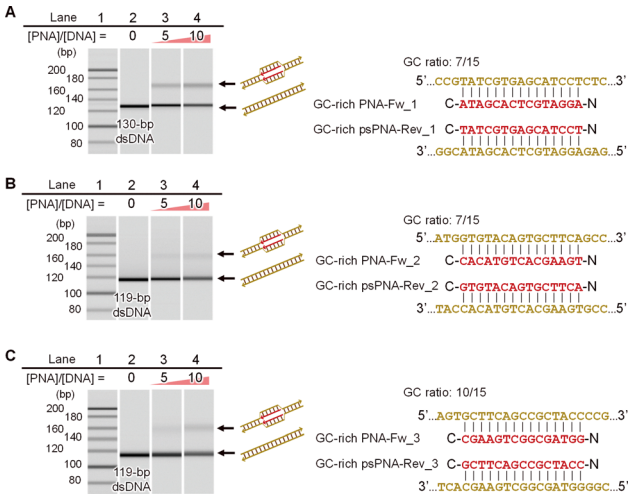

Fig. 7 EMSA demonstrated that the parallel-stranded PNA invasion system is adaptable to other DNA sequences. Lane 1: 20-bp DNA ladder marker; lane 2: 119 or 130-bp DNA only; lanes 3 and 4: GC-rich PNA-Fw_1 and GC-rich psPNA-Rev_1 for (A), GC-rich PNA-Fw_2 and GC-rich psPNA-Rev_2 for (B) and GC-rich PNA-Fw_3 and GC-rich psPNA-Rev_3 for (C). Invasion conditions: [DNA] = 100 nM, [each PNA] = 500–1000 nM (5–10 equiv. for DNA), and [HEPES (pH 7.0)] = 5 mM at 50 °C for 1 h.

significantly affected by the rate of parallel PNA/DNA duplex formation. In addition to conducting experiments at 50 °C, time-course studies were also performed at different temperatures (45 °C and 37 °C). The results indicated that the formation of the invasion complex was temperature-dependent, and the apparent activation energy (E_a) was calculated to be 161 kJ mol^{-1} from the corresponding k_{ps} values using an Arrhenius plot (Fig. 8C). The apparent activation energy for binding of parallel-stranded PNAs to DNA is closer to E_a = 150 kJ mol^{-1} obtained for double-duplex invasion by pcPNAs[31] than that for triplex invasion of homopyrimidine PNA (E_a = 58.4–79 kJ mol^{-1}).[49]

Compatibility of parallel design with pcPNAs

Importantly, parallel-stranded PNA invasion represents a fundamentally distinct strategy from approaches employing chemically modified PNAs, and thus, the parallel design is expected to be broadly compatible with existing PNA-based systems. To examine this compatibility, we incorporated pseudo-complementary nucleobases[15,30,33] as a model case to evaluate whether nucleobase modifications can be integrated into the parallel-stranded PNA framework. As shown in Fig. 9A, the introduction of two pseudo-complementary nucleobases into parallel-stranded PNAs significantly improved the invasion efficiency compared to the unmodified parallel design (lane 3, 52.2 ± 0.4% and lane 5, 92.4 ± 0.5%). These results demonstrate that nucleobase modifications can be effectively combined with parallel-stranded PNA invasion to enhance invasion efficiency. Interestingly, parallel-stranded PNAs containing pseudo-complementary nucleobases exhibited even higher invasion efficiency than the corresponding antiparallel pcPNAs (lane 4, 32.3 ± 1.5%), further supporting the effectiveness of the parallel PNA design in the context of sequence-specific dsDNA recognition.

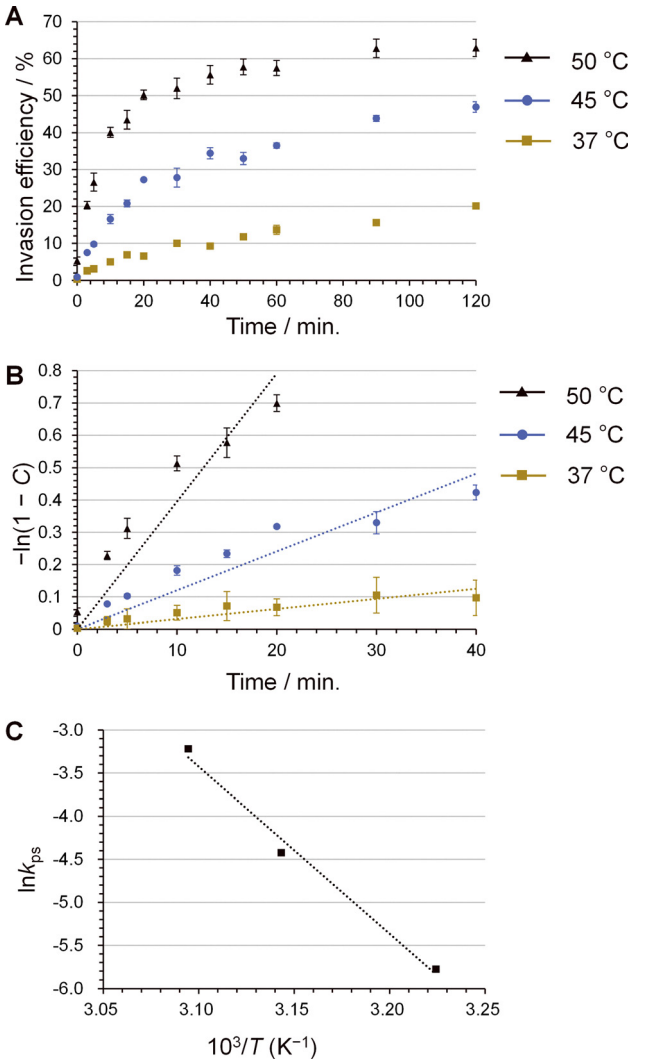

Fig. 8 (A) Time course plot of invasion complex formation. The fraction of the invasion complex was calculated based on the EMSA results. Invasion conditions: [DNA] = 100 nM, [each PNA] = 500 nM (5 equiv. for DNA), and [HEPES (pH 7.0)] = 5 mM, at 50, 45, and 37 °C. (B) Plot of $-\ln(1 - C)$ *versus* incubation time. $C = 1 - \exp(-k_{ps}t)$, where C is the fraction of the invasion complex at time t, and k_{ps} is the pseudo-first-order rate constant for parallel-stranded PNA invasion. (C) The Arrhenius plot of kinetic data for the binding of parallel-stranded PNAs to target dsDNA. The pseudo-first-order rate constants, k_{ps}, were determined from time-course measurements at different temperatures: k_{ps} (37 °C) = 3.1 × 10^{-3} min^{-1}, k_{ps} (45 °C) = 1.2 × 10^{-2} min^{-1}, and k_{ps} (50 °C) = 4.0 × 10^{-2} min^{-1}. The slope of the Arrhenius plot yielded an apparent activation energy (E_a) of 161 kJ mol^{-1}.

One of the major challenges in achieving double-duplex invasion using PNAs is the recognition of dsDNA under high-salt conditions, as increased ionic strength enhances the thermal stability of dsDNA, thereby hindering the formation of the invasion complex. Similar to observations with pcPNAs, parallel-stranded PNAs alone showed a decrease in invasion efficiency as the salt concentration increased (Fig. S7). However, the combination of the parallel design with pcPNA enabled invasion complex formation even under high-salt and molecular crowding conditions (Fig. 9B; lane 3, 5.3 ± 0.2%). These results demonstrate that various types of modified

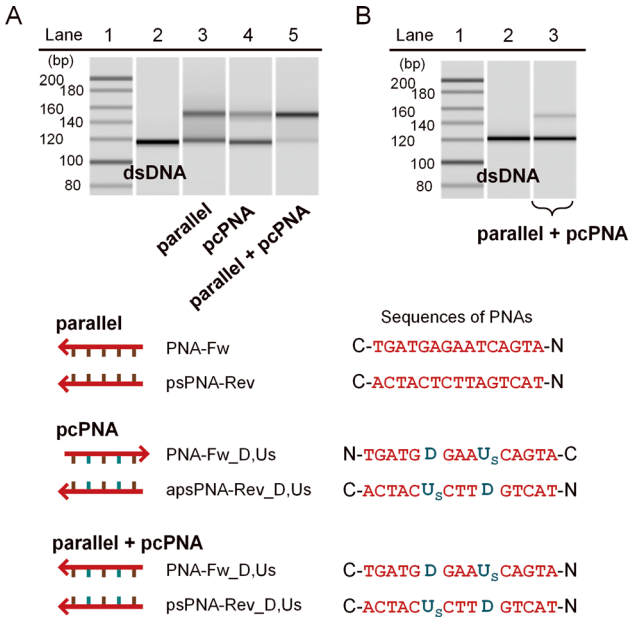

Fig. 9 (A) Enhancement of the invasion efficiency by combining parallel-stranded PNAs with pseudo-complementary nucleobases. Lane 1: DNA ladder marker; lane 2: 119-bp DNA only; lane 3: PNA-Fw and psPNA-Rev; lane 4: PNA-Fw_D,Us and apsPNA-Rev_D,Us; lane 5: PNA-Fw_D,Us and psPNA-Rev_D,Us. Invasion conditions: [DNA] = 100 nM, [each PNA] = 500 nM (5 equiv. for DNA), and [HEPES (pH 7.0)] = 5 mM at 50 °C for 1 h. (B) Parallel-stranded PNAs with pseudo-complementary nucleobases formed invasion complexes even under high salt and molecular crowding conditions. Lane 1: DNA ladder marker; lane 2: 119-bp DNA only; lane 3: PNA-Fw_D,Us and psPNA-Rev_D,Us. Invasion conditions: [DNA] = 200 nM, [each PNA] = 1000 nM (5 equiv. for DNA), [HEPES (pH 7.0)] = 5 mM, [NaCl] = 100 mM, [PEG 200] = 40% (w/v) at 37 °C for 15 h.

nucleobases,[46,47,50,51] beyond those used in pcPNAs, can be integrated into the parallel-stranded PNA system, offering a viable strategy for enhancing invasion efficiency. In standard pcPNAs, adenine and thymine are replaced with D and Us, respectively, which imposes a synthetic limitation that makes further chemical modification of AT bases challenging. The present findings highlight the versatility and utility of the parallel PNA design in invasion studies, as it is free from such structural constraints. Further studies on the functionalization of parallel-stranded PNAs may lead to improvements in sequence specificity, hybridization stability, and overall applicability of this approach. We anticipate that parallel PNA design will be established as a foundational strategy for dsDNA recognition and may ultimately be incorporated into a wider range of applications, including sequence-targeting technologies such as gene editing.

Conclusions

We focused on the unique ability of PNA to form parallel duplexes and demonstrated that strand-orientation-based design is highly effective for dsDNA recognition, particularly in the context of invasion complex formation. Rather than relying on nucleobase modifications, we achieved suppression of undesired PNA/PNA duplex formation, a critical requirement for efficient PNA invasion, by exploiting the thermodynamic differences associated with strand orientation. This approach, employing the less commonly utilized parallel-stranded configuration, facilitated sequence-selective dsDNA recognition and demonstrated the potential to recognize a broader range of sequences, including GC-rich targets. While chemical modification has long been considered indispensable for successful PNA invasion, our findings suggest that the use of parallel-stranded PNA offers an alternative route that may challenge this assumption. These results broaden our understanding of PNA binding modes to dsDNA and open up new avenues for PNA invasion strategies.

The concept of strand-orientation-based design is not limited to PNA but may also be applicable to other types of synthetic nucleic acids. The phenomenon of PNA invasion has attracted growing interest beyond PNA itself,[47,52,53] and since strand orientation is an inherent property of nucleic acids, the strategy proposed herein holds broad potential applicability. For example, innovative strategies,[9,54] such as the incorporation of intercalator moieties[55–58] or chemically reactive nucleobases,[59,60] have enabled invasion complex formation even in artificial nucleic acids with phosphate backbones. In these studies, as in the case of PNA, chemical modification has served as the predominant strategy for enabling invasion complex formation. In contrast, our parallel design introduces a novel conceptual perspective to the field, and we anticipate that this strategy will provide a promising platform for the development of diverse DNA recognition technologies using artificial nucleic acids.

Furthermore, we report the first crystal structure of a parallel PNA/PNA duplex. In the field of artificial nucleic acid research, attention has primarily been directed toward achieving high binding affinity, whereas parallel duplex structures—the focus of this study—have generally been considered suboptimal for practical use due to limited recognition performance. The fact that the parallel structure remained unexplored for 27 years following the initial report of the antiparallel duplex crystal structure illustrates the extent of this oversight.[34] The overall structure is similar to the P-type helix of the antiparallel PNA/PNA duplex, but importantly differences were observed in the coordination of surrounding water molecules. This crystal structure of parallel PNA/PNA duplex reported in this research is expected to provide a structural basis for the rational design of PNA derivatives,[4,5,61–69] as well as a major clue to elucidate the stability differences in the orientation of parallel and antiparallel PNA duplexes.

By leveraging the previously overlooked concept of parallel duplex formation, this study provides new insights and strategies for DNA recognition. The long-standing assumption that modified PNA derivatives are essential for successful PNA invasion may be reconsidered through the use of parallel-stranded PNA. These findings are expected to have a substantial impact not only on the field of PNA, but also on a broader range of synthetic nucleic acid research. In fact, parallel duplex formation has been reported for certain artificial nucleic acids

other than PNA.[70] While a few studies have highlighted the potential utility of parallel duplex formation,[71–73] this design principle remains largely underutilized in nucleic acid research. We believe that the findings presented in this study represent an important step toward establishing the utility of parallel architectures in nucleic acids and may serve as a milestone for the future development of nucleic acid-based technologies.

Author contributions

M. S. and Y. A. conceived the project. M. S. conducted all investigations and curated the data. H. S. also contributed to the crystallographic investigation and data curation. M. S. was responsible for visualization. The original draft was primarily written by M. S., with significant input from Y. A., and the manuscript was reviewed and edited by O. S., Y. A. and M. H. Project administration and funding acquisition were handled by O. S. and Y. A. The project was supervised jointly by O. S. and Y. A.

Conflicts of interest

There are no conflicts to declare.

Data availability

The data supporting this article have been included as part of the SI. See DOI: **https://doi.org/10.1039/d5cb00172b**

Crystallographic data have been deposited in the Protein Data Bank (PDB) under accession code 9L5Z.

Acknowledgements

This work was supported by JSPS KAKENHI grants [22K05350 to Y.A.; 22KJ1567 to M.S.; 22K21346 to O. S.] from the Ministry of Education, Culture, Sports, Science, and Technology (Japan). Additional support was provided by the Foundation of Public Interest of Tatematsu (Y. A.), the Noguchi Institute (Y. A.), and the Iwadare Scholarship (M. S.) from the Iwadare Scholarship Foundation. M. S. also gratefully acknowledges the support of the ''Nagoya University Interdisciplinary Frontier Fellowship'' funded by the Japan Science and Technology Agency (JST) and Nagoya University.

Notes and references

1 I. Anosova, E. A. Kowai, M. R. Dunn, J. C. Chaput, W. D. Van Horn and M. Egli, *Nucleic Acids Res.*, 2016, **44**, 1007–1021.
2 L. K. McKenzie, R. El-Khoury, J. D. Thorpe, M. J. Damha and M. Hollenstein, *Chem. Soc. Rev.*, 2021, **50**, 5126–5164.
3 H. Asanuma, Y. Kamiya, H. Kashida and K. Murayama, *Chem. Commun.*, 2022, **58**, 3993–4004.
4 A. Das and B. Pradhan, *Chem. Biol. Drug Des.*, 2021, **97**, 865–892.
5 C. Suparpprom and T. Vilaivan, *RSC Chem. Biol.*, 2022, **3**, 648–697.
6 P. E. Nielsen, M. Egholm, R. H. Berg and O. Buchardt, *Science*, 1991, **254**, 1497–1500.
7 P. Muangkaew and T. Vilaivan, *Bioorg. Med. Chem. Lett.*, 2020, **30**, 127064.
8 X. Liang, M. Liu and M. Komiyama, *Bull. Chem. Soc. Jpn.*, 2021, **94**, 1737–1756.
9 Y. Aiba, M. Shibata and O. Shoji, *Appl. Sci.*, 2022, **12**, 3677.
10 Y. Mikame and A. Yamayoshi, *Pharmaceutics*, 2023, **15**, 2515.
11 A. Sannigrahi, N. De, D. Bhunia and J. Bhadra, *Bioorg. Chem.*, 2025, **155**, 108146.
12 M. Egholm, O. Buchardt, L. Christensen, C. Behrens, S. M. Freier, D. A. Driver, R. H. Berg, S. K. Kim, B. Norden and P. E. Nielsen, *Nature*, 1993, **365**, 566–568.
13 S. M. Chen, V. Mohan, J. S. Kiely, M. C. Griffith and R. H. Griffey, *Tetrahedron Lett.*, 1994, **35**, 5105–5108.
14 P. E. Nielsen and L. Christensen, *J. Am. Chem. Soc.*, 1996, **118**, 2287–2288.
15 G. Haaima, H. F. Hansen, L. Christensen, O. Dahl and P. E. Nielsen, *Nucleic Acids Res.*, 1997, **25**, 4639–4643.
16 S. Rapireddy, G. He, S. Roy, B. A. Armitage and D. H. Ly, *J. Am. Chem. Soc.*, 2007, **129**, 15596–15600.
17 Y. Aiba, Y. Yamamoto and M. Komiyama, *Chem. Lett.*, 2007, **36**, 780–781.
18 G. F. He, S. Rapireddy, R. Bahal, B. Sahu and D. H. Ly, *J. Am. Chem. Soc.*, 2009, **131**, 12088–12090.
19 Y. Aiba, Y. Hamano, W. Kameshima, Y. Araki, T. Wada, A. Accetta, S. Sforza, R. Corradini, R. Marchelli and M. Komiyama, *Org. Biomol. Chem.*, 2013, **11**, 5233–5238.
20 N. Shigi, Y. Mizuno, H. Kunifuda, K. Matsumura and M. Komiyama, *Bull. Chem. Soc. Jpn.*, 2019, **92**, 330–335.
21 D. Y. Cherny, B. P. Belotserkovskii, M. D. Frank-Kamenetskii, M. Egholm, O. Buchardt, R. H. Berg and P. E. Nielsen, *Proc. Natl. Acad. Sci. U. S. A.*, 1993, **90**, 1667–1670.
22 M. Egholm, L. Christensen, K. L. Dueholm, O. Buchardt, J. Coull and P. E. Nielsen, *Nucleic Acids Res.*, 1995, **23**, 217–222.
23 H. Kuhn, V. V. Demidov, J. M. Coull, M. J. Fiandaca, B. D. Gildea and M. D. Frank-Kamenetskii, *J. Am. Chem. Soc.*, 2002, **124**, 1097–1103.
24 T. Bentin, H. J. Larsen and P. E. Nielsen, *Biochemistry*, 2003, **42**, 13987–13995.
25 K. Kaihatsu, R. H. Shah, X. Zhao and D. R. Corey, *Biochemistry*, 2003, **42**, 13996–14003.
26 A. S. Ricciardi, R. Bahal, J. S. Farrelly, E. Quijano, A. H. Bianchi, V. L. Luks, R. Putman, F. Lopez-Giraldez, S. Coskun, E. Song, Y. F. Liu, W. C. Hsieh, D. H. Ly, D. H. Stitelman, P. M. Glazer and W. M. Saltzman, *Nat. Commun.*, 2018, **9**, 2481.
27 M. Lyu, L. Kong, Z. Yang, Y. Wu, C. E. McGhee and Y. Lu, *J. Am. Chem. Soc.*, 2021, **143**, 9724–9728.
28 A. S. Piotrowski-Daspit, C. Barone, C. Y. Lin, Y. X. Deng, D. G. Wu, T. C. Binns, E. M. Y. Xu, A. S. Ricciardi, R. Putman, A. Garrison, R. Nguyen, A. Gupta, R. Fan,

P. M. Glazer, W. M. Saltzman and M. E. Egan, *Sci. Adv.*, 2022, **8**, eabo0522.
29 B. R. Tessier and E. Rozners, *Chem. Commun.*, 2025, **61**, 4070–4073.
30 J. Lohse, O. Dahl and P. E. Nielsen, *Proc. Natl. Acad. Sci. U. S. A.*, 1999, **96**, 11804–11808.
31 V. V. Demidov, E. Protozanova, K. I. Izvolsky, C. Price, P. E. Nielsen and M. D. Frank-Kamenetskii, *Proc. Natl. Acad. Sci. U. S. A.*, 2002, **99**, 5953–5958.
32 P. Wittung, P. E. Nielsen, O. Buchardt, M. Egholm and B. Norden, *Nature*, 1994, **368**, 561–563.
33 M. Komiyama, Y. Aiba, T. Ishizuka and J. Sumaoka, *Nat. Protoc.*, 2008, **3**, 646–654.
34 H. Rasmussen, J. S. Kastrup, J. N. Nielsen, J. M. Nielsen and P. E. Nielsen, *Nat. Struct. Biol.*, 1997, **4**, 98–101.
35 J. I. Yeh, E. Pohl, D. Truan, W. He, G. M. Sheldrick, S. Du and C. Achim, *Chem. – Eur. J.*, 2010, **16**, 11867–11875.
36 H. Kuhn, D. I. Cherny, V. V. Demidov and M. D. Frank-Kamenetskii, *Proc. Natl. Acad. Sci. U. S. A.*, 2004, **101**, 7548–7553.
37 M. Hibino, Y. Aiba, Y. Watanabe and O. Shoji, *ChemBioChem*, 2018, **19**, 1601–1604.
38 M. Egholm, C. Behrens, L. Christensen, R. H. Berg, P. E. Nielsen and O. Buchardt, *J. Chem. Soc., Chem. Commun.*, 1993, 800–801.
39 K. K. Jensen, H. Ørum, P. E. Nielsen and B. Nordén, *Biochemistry*, 1997, **36**, 5072–5077.
40 G. L. Igloi, *Proc. Natl. Acad. Sci. U. S. A.*, 1998, **95**, 8562–8567.
41 T. Ratilainen, A. Holmen, E. Tuite, P. E. Nielsen and B. Norden, *Biochemistry*, 2000, **39**, 7781–7791.
42 W. He, E. Hatcher, A. Balaeff, D. N. Beratan, R. R. Gil, M. Madrid and C. Achim, *J. Am. Chem. Soc.*, 2008, **130**, 13264–13273.
43 J. I. Yeh, B. Shivachev, S. Rapireddy, M. J. Crawford, R. R. Gil, S. Du, M. Madrid and D. H. Ly, *J. Am. Chem. Soc.*, 2010, **132**, 10717–10727.
44 T. Ishizuka, J. Yoshida, Y. Yamamoto, J. Sumaoka, T. Tedeschi, R. Corradini, S. Sforza and M. Komiyama, *Nucleic Acids Res.*, 2008, **36**, 1464–1471.
45 A. G. Olsen, O. Dahl, A. B. Petersen, J. Nielsen and P. E. Nielsen, *Artif. DNA: PNA XNA*, 2011, **2**, 32–36.
46 M. Hibino, Y. Aiba and O. Shoji, *Chem. Commun.*, 2020, **56**, 2546–2549.
47 M. López-Tena, L. Farrera-Soler, S. Barluenga and N. Winssinger, *JACS Au*, 2023, **3**, 449–458.
48 D. J. Rose, *Anal. Chem.*, 1993, **65**, 3545–3549.
49 P. Wittung, P. Nielsen and B. Nordén, *J. Am. Chem. Soc.*, 1996, **118**, 7049–7054.
50 S. S. Moriya, H. Shibasaki, M. Kohara, K. Kuwata, Y. Imamura, Y. Demizu, M. Kurihara, A. Kittaka and T. Sugiyama, *Bioorg. Med. Chem. Lett.*, 2021, **39**, 127850.
51 S. S. Moriya, K. Funaki, Y. Demizu, M. Kurihara, A. Kittaka and T. Sugiyama, *Bioorg. Med. Chem. Lett.*, 2023, **88**, 129287.
52 N. Yotapan, D. Nim-anussornkul and T. Vilaivan, *Tetrahedron*, 2016, **72**, 7992–7999.
53 S. A. Thadke, V. M. Hridya, J. D. R. Perera, R. R. Gil, A. Mukherjee and D. H. Ly, *Commun. Chem.*, 2018, **1**, 79.
54 E. M. Zaghloul, A. S. Madsen, P. M. D. Moreno, I. I. Oprea, S. El-Andaloussi, B. Bestas, P. Gupta, E. B. Pedersen, K. E. Lundin, J. Wengel and C. I. E. Smith, *Nucleic Acids Res.*, 2011, **39**, 1142–1154.
55 D. C. Guenther, G. H. Anderson, S. Karmakar, B. A. Anderson, B. A. Didion, W. Guo, J. P. Verstegen and P. J. Hrdlicka, *Chem. Sci.*, 2015, **6**, 5006–5015.
56 H. Asanuma, R. Niwa, M. Akahane, K. Murayama, H. Kashida and Y. Kamiya, *Biorg. Med. Chem.*, 2016, **24**, 4129–4137.
57 C. P. Shepard, R. G. Emehiser, S. Karmakar and P. J. Hrdlicka, *Molecules*, 2023, **28**, 127.
58 M. E. Everly, R. G. Emehiser and P. J. Hrdlicka, *Org. Biomol. Chem.*, 2025, **23**, 619–628.
59 S. Nakamura, H. Kawabata and K. Fujimoto, *Chem. Commun.*, 2017, **53**, 7616–7619.
60 S. Sethi, H. Zumila, Y. Watanabe, J. Mo and K. Fujimoto, *Bioorg. Med. Chem. Lett.*, 2024, **98**, 129597.
61 K. L. Dueholm, K. H. Petersen, D. K. Jensen, M. Egholm, P. E. Nielsen and O. Buchardt, *Bioorg. Med. Chem. Lett.*, 1994, **4**, 1077–1080.
62 S. Sforza, G. Haaima, R. Marchelli and P. E. Nielsen, *Eur. J. Org. Chem.*, 1999, 197–204.
63 M. D'Costa, V. A. Kumar and K. N. Ganesh, *Org. Lett.*, 1999, **1**, 1513–1516.
64 A. Dragulescu-Andrasi, S. Rapireddy, B. M. Frezza, C. Gayathri, R. R. Gil and D. H. Ly, *J. Am. Chem. Soc.*, 2006, **128**, 10258–10267.
65 T. Sugiyama, Y. Imamura, Y. Demizu, M. Kurihara, M. Takano and A. Kittaka, *Bioorg. Med. Chem. Lett.*, 2011, **21**, 7317–7320.
66 T. Bose, A. Banerjee, S. Nahar, S. Maiti and V. A. Kumar, *Chem. Commun.*, 2015, **51**, 7693–7696.
67 P. Sriwarom, P. Padungros and T. Vilaivan, *J. Org. Chem.*, 2015, **80**, 7058–7065.
68 H. Zheng, I. Botos, V. Clausse, H. Nikolayevskiy, E. E. Rastede, M. F. Fouz, S. J. Mazur and D. H. Appella, *Nucleic Acids Res.*, 2021, **49**, 713–725.
69 M. López-Tena, E. E. Watson, P. Romanens and N. Winssinger, *Helv. Chim. Acta*, 2023, **106**, e202300110.
70 H. Kashida, K. Murayama, T. Toda and H. Asanuma, *Angew. Chem., Int. Ed.*, 2011, **50**, 1285–1288.
71 A. Accetta, A. G. Petrovic, R. Marchelli, N. Berova and R. Corradini, *Chirality*, 2015, **27**, 864–874.
72 P. Kulkarni, D. Datta and K. N. Ganesh, *ACS Omega*, 2022, **7**, 40558–40568.
73 C. Terada, K. Oh, R. Tsubaki, B. Chan, N. Aibara, K. Ohyama, M. A. Shibata, T. Wada, M. Harada-Shiba, A. Yamayoshi and T. Yamamoto, *Nat. Commun.*, 2023, **14**, 7972.